Spin-rotation parameters A and R for π^+p and π^-p elastic scattering from 427 to 657 MeV/c

I. Supek,[a,*] D. B. Barlow,[b,†] W. J. Briscoe,[c] J. F. Davis,[d] G. J. Kim,[b,‡] D. W. Lane,[a]
A. Mokhtari,[c] B. M. K. Nefkens,[b] C. Pillai,[b,†] M. E. Sadler,[a] C. J. Seftor,[c] M. F. Taragin,[c] and J. A. Wightman[b,§]
[a]*Abilene Christian University, Abilene, Texas 79699*
[b]*University of California, Los Angeles, California 90024*
[c]*George Washington University, Washington, D.C. 20052*
[d]*Los Alamos National Laboratory, Los Alamos, New Mexico 87545*
(Received 26 February 1992)

The spin-rotation parameters A and R and the related spin-rotation angle β have been measured for π^+p and π^-p elastic scattering using protons polarized in the scattering plane. The pion-beam momenta are 427, 471, 547, 625, and 657 MeV/c and the angular range is $-0.9 \leq \cos\Theta_{\text{c.m.}} \leq 0.3$. The scattered pion and recoil proton were detected in coincidence, using a scintillator hodoscope for the pions, and the Large Acceptance Spectrometer combined with the JANUS polarimeter for the recoil protons. The results are compared with the four recent πN partial wave analyses (PWA's). Our data show that the major features of these PWA's are correct. The A and R measurements complete our program of pion-nucleon experiments, providing full data sets at three of the above beam momenta. Such sets can be used to test the constraints in the PWA's or to obtain a model-independent set of πN scattering amplitudes.

PACS number(s): 13.75.Gx, 13.88.+e

I. INTRODUCTION

We report the measurement of the two components of the recoil proton polarization in the scattering plane for π^- and π^+ elastic scattering on a proton target that is polarized in the scattering plane. The present data were obtained at $P_{\text{lab}}=427$, 471, 547, 625, and 657 MeV/c. The results are presented in terms of the Wolfenstein spin rotation parameters A and R, as well as the spin rotation angle β. This experiment completes a series of pion-nucleon experiments which were performed at LAMPF by the UCLA-ACU-GWU Collaboration. The aim is to obtain model-independent pion-nucleon scattering amplitudes. Previous measurements include $d\sigma/d\Omega$ and A_N for elastic scattering, $\pi^{\pm}p \rightarrow \pi^{\pm}p$ [1–3], and, for charge exchange, $\pi^-p \rightarrow \pi^0n$ [4–6]. For the first time ever there exists a complete set of measurements on the basic πN system over an extended angle and momentum interval (i.e., 471, 547, and 625 MeV/c beam momenta). Actually, the total number of measured parameters is ten and only eight are necessary to determine fully the scattering amplitudes at a single energy [7].

A complete data set may be used to determine directly the πN scattering amplitudes, save for a common phase factor. Until now, these amplitudes have been deduced from partial wave analysis (PWA) of incomplete πN data sets relying on theoretical constraints. The most recent analyses of π^+p and π^-p scattering covering an extended energy interval in the resonance region have been made by groups from the Virginia Polytechnic Institute (VPI) [8], Karlsruhe-Helsinki (KH) [9], Carnegie-Mellon University and Lawrence Berkeley Laboratory (CL) [10], and Leningrad (now St. Petersburg) [11]. The constraints common to these analyses are based on unitarity, isospin invariance and forward dispersion relations. The KH and CL groups have obtained a unique solution by using additional constraints that result from dispersion relations derived from the Mandelstam hypothesis that the amplitudes are analytic functions of the variables s and t. The four analyses differ in the treatment of electromagnetic effects, in the procedure in which the theoretical constraints are applied, in the parametrization of the data and in the experimental data bases. The Particle Data Group's [12] compilation of N and Δ baryon resonances is based on the KH and CL analyses, each of which was last updated in 1980. The KH analysis extends to 10 GeV/c and the CL to 2.5 GeV/c. The update of the Karlsruhe analysis to include our data and those of other collaborations is in progress. The parametrization used by the VPI group gives the flexibility of updating the analysis periodically via the SAID facility in the momentum region below 2.1 GeV/c.

In the energy range of our measurements there are two resonances: the $\Delta(1232)$ (P_{33}) and the $N(1440)$ (P_{11}), sometimes called the Roper resonance. The P_{11} has the same quantum numbers as the nucleon and various phenomenological analyses and theoretical models disagree on the parameters of this resonance. The KH group gives the following values: mass $M=1410\pm12$ MeV, width $\Gamma=135\pm10$ MeV and inelasticity $\eta=0.51\pm0.05$; the CL PWA obtained $M=1440\pm30$ MeV, $\Gamma=340\pm70$ MeV, and $\eta=0.68\pm0.04$; while the most recent VPI

*Permanent address: Rudjer Boskovic Institute, 41000 Zagreb, Croatia.
†Present address: Los Alamos National Laboratory, Los Alamos, NM 87545.
‡Present address: Cyclotron Institute, Texas A&M University, College Station, TX 77843.
§Present address: Texas A&M University, College Station, TX 77843.

article reported two poles in the complex plane for the P_{11} channel at $P(\mathrm{I})=(1359-100i)$ MeV and $P(\mathrm{II})=(1410-80i)$ MeV. The occurrence of multiple poles on different Riemann sheets in the presence of coupled channels has been predicted by Eden and Taylor [13]. In this case, the P_{11} occurs between the opening of the $\pi\Delta$ and ηN channels. The question arises whether the second pole is a physically distinct state (resonance) or is a shadow pole. Cutkosky and Wang [14] addressed this question and concluded that "the difference in resonance structure reported by CL and VPI arises from the different parametrization used, rather than from differences in the data." The phenomenon is physically interesting since it provides a mechanism to study shadow poles for an isolated resonance. An example of a shadow pole in a nuclear system has been reported for the $J^\pi=\frac{3}{2}^+$ resonance in ^{5}He [15].

The theoretical calculations also differ in their predictions for the P_{11} resonance. The quark model of Karl, Isgur, and Koniuk (KIK) [16] predicts the mass of the Roper resonance to be $M=1405$ MeV. Two of the many QCD-inspired models based on a bag-model calculation predict the existence of a ground-state Q^3G hybrid with a mass around 1400 MeV in the vicinity of the three-quark P_{11} resonance with $M=1440$ MeV [17]. The Skyrme or chiral soliton model [18] calculates πN amplitudes without the use of the underlying quark structure and finds novel relations between the isospin $\frac{1}{2}$ and $\frac{3}{2}$ amplitudes.

II. πN SCATTERING FORMALISM

A. Pion-nucleon elastic scattering

The complete amplitude M describing the elastic scattering of a spin-0 projectile on a spin-$\frac{1}{2}$ target, can be decomposed into two independent components as a consequence of rotational invariance and parity. These components are usually chosen to be the spin-nonflip $f(\theta)$ and the spin-flip $g(\theta)$ amplitudes. We have

$$M=f+ig\mathbf{n}\cdot\boldsymbol{\sigma} , \tag{1}$$

with

$$\mathbf{n}=(\mathbf{k}_i\times\mathbf{k}_f)/|\mathbf{k}_i\times\mathbf{k}_f| , \tag{2}$$

which is the normal to the scattering plane, the σ's are the Pauli spin matrices, $\mathbf{k}_i$ and $\mathbf{k}_f$ are initial and final proton momentum in the c.m., and θ is the c.m. scattering angle. The differential cross section is

$$I=|f|^2+|g|^2 . \tag{3}$$

The transverse polarization P of the recoil proton is given by

$$P=2\,\mathrm{Im}(fg^*)/I . \tag{4}$$

When the experimental data are limited to I and P, the two eigenstates of M have an ambiguity in their relative phase except at 0° and 180°. This is clear as I and P are invariant under the transformation

$$(f\pm ig)\rightarrow e^{\mp i\tau/2}(f\pm ig) . \tag{5}$$

This ambiguity can be resolved by a measurement of the spin-rotation parameters in elastic pion scattering on protons polarized in the scattering plane.

The components of the proton polarization in the laboratory scattering plane are defined in Fig. 1. The spin-rotation parameters are defined [19] and the sign convention used [20] is such that the initial P_i and final P_f polarizations in the scattering plane are related by

$$S_f=-AL_i-RS_i , \tag{6a}$$

$$L_f=-RL_i+AS_i . \tag{6b}$$

Experimentally, A and R can be determined by measuring the components of the recoil proton polarization along $\mathbf{s}_f$ and $\mathbf{l}_f$, respectively, from a target that is polarized in the same plane. The final polarization, $\mathbf{P}_f$, of the recoil proton in the laboratory frame is given by

$$\mathbf{P}_f=AP_i\mathbf{s}_f+P\mathbf{n}+RP_i\mathbf{l}_f , \tag{7}$$

where P is the component of the recoil proton's polarization normal to the scattering plane. In terms of the above scattering amplitudes, A, R, and β [21] are given by

$$AI=(|f|^2-|g|^2)\sin\theta_L+2\,\mathrm{Re}(fg^*)\cos\theta_L , \tag{8a}$$

$$RI=(|f|^2-|g|^2)\cos\theta_L-2\,\mathrm{Re}(fg^*)\sin\theta_L , \tag{8b}$$

$$\beta=-\arctan(-A/R)+\theta+\theta_L+n360^\circ , \tag{8c}$$

where θ_L is the laboratory angle of the recoil proton and n is an integer. From their definition, it is immediately clear that the polarization parameters A, R, and P obey the identity

$$A^2+R^2+P^2=1 . \tag{9}$$

The validity of this relation depends only on conservation of parity and rotational invariance. It follows from Eqs. (8c) and (9) that the spin-rotation angle has a singularity when $P=\pm1$ because A and R must be zero.

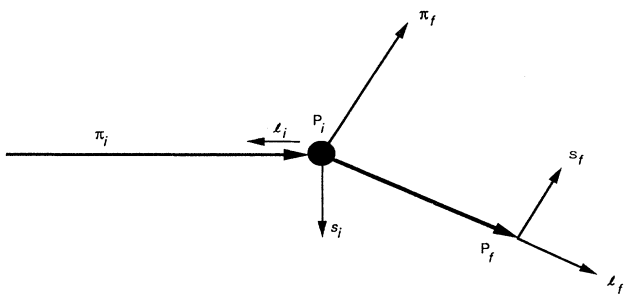

FIG. 1. The definition of the proton polarization components in the laboratory scattering plane, where P_i is initial and P_f final polarization.

B. Test of isospin invariance

Complete data sets for the πN system can be used to test isospin invariance of the strong interaction [22]. Isospin invariance implies that the πN interaction depends on only two isospin amplitudes ($I=\frac{1}{2},\frac{3}{2}$), where the decomposition into these independent amplitudes is given by appropriate Clebsch-Gordan coefficients. Three different reactions can be observed in πN elastic scattering, namely, $\pi^+p\to\pi^+p$, $\pi^-p\to\pi^-p$, and $\pi^-p\to\pi^0n$.

Figure 2, adopted from Ref. [22], shows how isospin invariance can be tested if the differential cross section I and transverse polarization P are measured for all three reactions and the spin-rotation angles $\beta+$ and $\beta-$ are measured for $\pi^+p\to\pi^+p$ and $\pi^-p\to\pi^-p$. The squares of the magnitudes of the transversity amplitudes, $|F(\pm)|^2$, are determined from the scattering observables by

$$|F(\pm)|^2=I(1\pm P)\ . \tag{10}$$

The combination using the plus sign is commonly called the transversity-up amplitude and the one with the minus sign is called the transversity-down amplitude. The subscripts used for $F(\pm)$ in Fig. 2 correspond to the different charge states of the reaction. $F_+(+)$ is the transversity-up amplitude for $\pi^+p\to\pi^+p$, $F_0(+)$ is the transversity-up amplitude for $\pi^-p\to\pi^0n$, etc. Finally, the interdependence of the scattering amplitudes for the three reactions (shown in Fig. 2) is

$$F_0(\pm)=\frac{F_+(\pm)-F_-(\pm)}{\sqrt{2}}\ , \tag{11}$$

forming two triangles in isospin space. Knowing the magnitudes (determined from experimental data) of all three of these amplitudes allows one to determine the angle $\gamma(+)$ between $F_+(+)$ and $F_-(+)$. A similar determination is possible for $\gamma(-)$ using the transversity-down amplitudes. The relative orientations of the two transversity amplitudes for π^+p scattering is β_+, and for π^-p scattering is β_-, see Fig. 2. Finally, isospin invariance can be tested using the relation

$$\beta_+-\beta_-=\pm\gamma(+)\pm\gamma(-)\ , \tag{12}$$

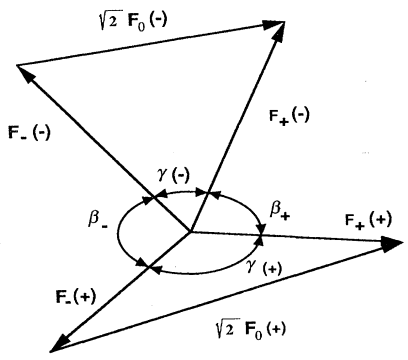

FIG. 2. The scattering amplitudes in isospin space.

if I and P are known for all three reactions and β_+ and β_- for the elastic reactions at a given energy and angle. The sign ambiguities are a consequence of being able to determine only the magnitudes of $F_{+,-,0}$ from experimental data. The numerical details of this test based on these data will be presented in a separate publication.

III. THE EXPERIMENT

A. Determination of A, R, and β

In this experiment A and R are measured simultaneously. This is possible because we used a detection system in which the recoil proton spin is precessed in the plane normal to the scattering plane. We used the dipole magnet of the Large Acceptance Spectrometer (LAS) to bend the recoil proton upwards. The precession angle of the proton spin relative to the momentum vector is given by

$$\theta_R=\gamma\theta_b(\tfrac{1}{2}g-1)\ , \tag{13}$$

where γ is the Lorentz factor, θ_b is the recoil proton bend angle in the LAS, and $g=5.5856$ is the proton Landé factor. To achieve $\theta_R=90°$, we need $\theta_b=50.2°/\gamma$ which is close to the nominal bend angle of 45°. The bend angle was reduced to 42° in this experiment which is a compromise over the range of optimal bend angles 38°–45°. Therefore, the recoil proton polarization components which were initially along l_f and s_f are now oriented in a plane normal to its momentum. The polarization, $\mathbf{P}_J$, measured by the JANUS polarimeter is related to the recoil proton polarizations by the spin precession matrix B, which is the average precession of the proton spins traversing the magnetic fields of target and LAS:

$$\mathbf{P}_J=B\mathbf{P}_f \tag{14a}$$

or

$$\begin{bmatrix}S_J\\N_J\\L_J\end{bmatrix}=\begin{bmatrix}b_{11}&b_{12}&b_{13}\\b_{21}&b_{22}&b_{23}\\b_{31}&b_{32}&b_{33}\end{bmatrix}\begin{bmatrix}S_f\\N_f\\L_f\end{bmatrix}\ , \tag{14b}$$

where S_J and N_J are polarization components measured by the JANUS polarimeter. The target assembly was rotated in the scattering plane by an angle θ_H (a positive θ_H is a rotation of the target toward the LAS). The components of the initial polarization become

$$S_i=P_t^{\pm}\sin\theta_H \quad\text{and}\quad L_i=-P_t^{\pm}\cos\theta_H\ , \tag{15}$$

where P_t^+ is the absolute target polarization for the case when the protons are polarized in the forward scattering plane and P_t^- is the opposite target polarization. The up-down asymmetries ($\epsilon_{\rm UD}=S_J A_C$, where A_C is carbon analyzing power) and left-right asymmetries ($\epsilon_{\rm LR}=N_J A_C$) measured by the polarimeter for each target polarization, can be calculated by substitution of Eqs. (6) and (15) in the first two rows of (14), and we have

$$S_J = b_{11}P_t^{\pm}[A(\pm)\cos\theta_H - R(\pm)\sin\theta_H] + b_{12}N_f + b_{13}P_t^{\pm}[R(\pm)\cos\theta_H + A(\pm)\sin\theta_H] , \quad (16a)$$

$$N_J = b_{21}P_t^{\pm}[A(\pm)\cos\theta_H - R(\pm)\sin\theta_H] + b_{22}N_f + b_{23}P_t^{\pm}[R(\pm)\cos\theta_H + A(\pm)\sin\theta_H] , \quad (16b)$$

where $A(+)$ and $R(+)$ correspond to P_t^+ and $A(-)$ and $R(-)$ correspond to P_t^-. The transverse component of the polarization P is equal to the analyzing power A_N obtained using a transversely polarized target [23]. A_N was obtained from a polynomial fit to the A_N data obtained in a previous experiment by the UCLA-GWU-ACU Collaboration [2]. Therefore, Eqs. (16) can be solved for $A(+)$, $A(-)$, $R(+)$, and $R(-)$. By averaging $A(+)$ and $A(-)$ or $R(+)$ and $R(-)$ the final value of A or R parameter is obtained. For the ideal case of a target polarized along the beam direction ($\theta_H = 0$) and for 90° spin precession, A is given by up-down scattering asymmetry in the polarimeter, while the left-right asymmetry yields R.

The spin precession matrix B was obtained from a Monte Carlo simulation of the experiment which tracks the recoil protons through the apparatus. The selection of the incident pion from the given phase space, the interaction point in the target, and the scattering angle are made randomly within appropriate ranges. The simulation also included energy loss, multiple scattering in the target, geometric constraints, and the magnetic fields. The relativistic equations of motion and polarization precession were integrated using a classical fourth-order Runge-Kutta method with the proper time of each particle as the integration variable. Detailed particle histories were kept for every event. A few sections were checked by hand and graphical displays were used to check for gross errors. It was estimated that the end point of a typical simulated recoil proton track was within a millimeter of its ideal position. The uncertainties due to the magnetic-field approximations are on the order of a centimeter. Path differences of this magnitude have negligible effect on the spin precession of the recoil proton and the dominant uncertainty is due to the statistics of the Monte Carlo simulation.

B. Experimental setup

The experiment was run at LAMPF in the P^3 (pion and particle physics) channel. The total beam time was about 1600 h. The experimental arrangement involves three essential components: (1) an intense pion beam ($>10^6$ π/s), (2) a proton target polarized in the scattering plane, and (3) a proton polarimeter.

The P^3 channel provides negative or positive pions in the momentum range from 190 to about 700 MeV/c [24]. The pion beam was typically 1 cm in diameter at the target with a momentum bit of 0.5–2.0 %. The beam intensity was 10^6–10^8 π/s. Two muon telescopes located upstream of the target in the beam halo were used to measure the relative beam intensity by detecting muons from decay of pions in flight. Two LAMPF beam-profile monitors [25] (BPM-1 and BPM-2) located 30 cm upstream and downstream of the target were used to focus and monitor the beam. The experimental setup is shown in Fig. 3.

The target cell was a 5-cm-long cylinder 2 cm in diameter, filled with propanediol (CH_3-$CHOH$-CH_2OH) beads of about 1 mm diam. The target cell was located in a target insert placed inside the cryostat. The use of the target insert made it possible to load the target at liquid-nitrogen temperature. Inside the insert was a waveguide, through which microwave energy was fed to the target. The target was cooled by two separated systems: a ^{4}He refrigerator and a ^{3}He-^{4}He dilution refrigerator. A superconducting split-coil magnet, the DESY ep collider HERA [26], provided a uniform magnetic field over the target volume (better than ±0.01%). This magnet was cooled in a liquid ^{4}He bath. The target polarization was

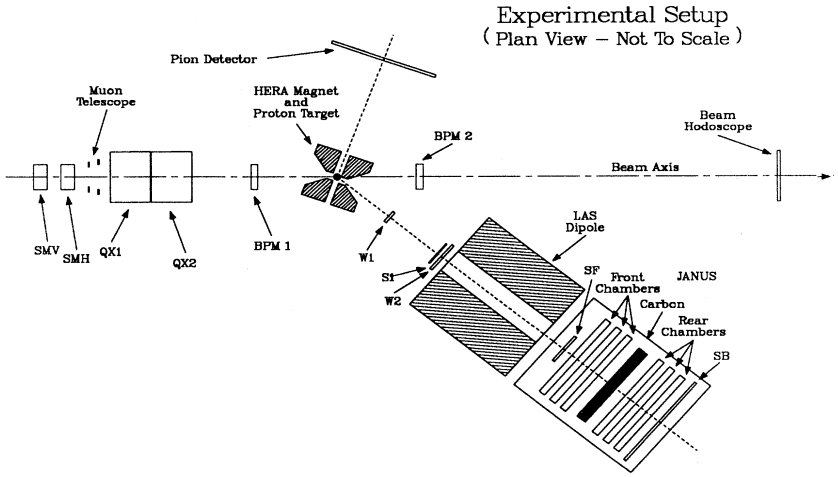

FIG. 3. Plan view of the experimental setup.

measured by nuclear magnetic resonance (NMR) technique. The "forbidden transition" method [27] was employed to polarize the target using microwaves of a suitable frequency to transfer the resultant electron polarization to the hydrogen nuclei. This occurs through a strong dipolar interaction in the 2.5 T magnetic field of HERA at a temperature of 0.5 K. When a satisfactory nuclear polarization was obtained (75–85 %), the temperature of the target material was lowered below 0.05 K. At this temperature the nuclear spins are frozen and the microwave power can be switched off and the magnetic field reduced to 0.5 T. This was essential in order to reduce the bending of the charged particles. The typical nuclear relaxation times ranged from 100 to 700 h [28]. The relaxation times were shorter on average for π^+ beams, due to increased energy deposition in the target from the higher intensities and proton contamination. The proton polarization direction was reversed periodically.

The gap between the Helmholtz coils of the HERA magnet provided a horizontal opening angle of $\pm 7°$ and a vertical opening of $\pm 20°$ (see Fig. 3). The support system for the HERA magnet and target cryogenics was modified to allow the rotation of the HERA axis from $-10°$ to $+20°$ with respect to the incident beam so that the scattered particles were not intercepted by the superconducting coils or the support assembly. Thus, the detection of pions and protons in coincidence was possible in the center-of-mass angular range from 95° to 120° for the "sideways" configuration (pions exit through the side opening), and from 130° to 145° for the "backward" configuration (recoil protons exit through the front HERA cone and the pions through the back one).

The proton detection system included the modified LAS [29] and the JANUS polarimeter [30] mounted on a frame on wheels which was pivoted around the target. Two LAS wire chambers were used to determine the trajectory of the recoil proton. In the front of a second LAS chamber a scintillator detector $S1$ was located. The dipole magnet of the LAS bent the recoil protons in the plane normal to the scattering plane. The polarimeter consisted of a front scintillator (FS), an upstream set of three delay-line wire chambers, a carbon analyzer, a downstream set of three wire chambers, and two double ended back scintillators (BS's). The thickness of carbon could be varied from 3.2 to 9.6 cm. The active area of the wire chambers was 60 cm$\times$60 cm, and the spatial resolution was better than 1 mm.

The pion hodoscope consisted of a double array of overlapping plastic scintillators arranged in two adjacent planes; it was installed on a cart. The front plane consisted of nine horizontal scintillators and the rear one of seven vertical scintillators. The scintillators were 14 cm wide and overlapped with their neighboring scintillators by $\frac{1}{3}$ of their width. A horizontal and vertical resolution of about 5 cm was achieved.

The electronics were set up in a coincidence configuration to select pion-proton elastic scattering events. The good event trigger was defined by a coincidence between three planes of the scintillators ($S1$, FS, BS) of the recoil proton detector and the pion hodoscope. No additional restrictions were imposed on the data which were written to tape. The scintillators in the front and rear of JANUS provided additional timing information.

IV. DATA ANALYSIS

A. Tests

Various tests and cuts were applied to obtain a clean sample of events. The tests that have physical significance are described below. First, each set of chambers was checked independently to eliminate multiple hits or rescattered secondary particles. This was done by requiring the proper value for the sum of the delay-line-end times for each chamber and by requiring the track through a set of three chambers to lie along a straight line. In the next stage, the good events in JANUS were determined by checking the consistency of the tracks recorded by two sets of chambers. The event was rejected if the distance of closest approach between the trajectories (DCLOSE), as determined by the front and rear chambers, was greater than 2.5 mm or occurred outside the carbon scatterer. That could be the case if the front and rear chambers had recorded trajectories of two different events or if the proton scattered more than once in the carbon analyzer. Proton trajectories with a scattering angle smaller than 3.4° were excluded because they are mainly produced by multiple Coulomb scattering. Also, a test on the azimuthal scattering angle Φ insured that for any event with a given Φ the possible event with $\Phi+\pi$ could also be accepted within the geometry of the spectrometer. The majority of taped events were eliminated by these cuts. Furthermore, protons that were accepted by the LAS were tested for correct momentum (PMOM) and time of flight (TOF). The trajectory determined by the LAS wire chambers was traced back to the target to ensure acceptance of particles that originated in the target cell. Finally, kinematics ($\theta_P+\theta_\pi \simeq 180°$) and coplanarity tests ($\Phi_P-\Phi_\pi \simeq 0$) were applied so that only elastically scattered events were accepted. These tests were also used to determine the background due to quasi-elastic scattering as explained below. A typical example of a coplanarity histogram is shown in Fig. 4. Markers 2 and 3 indicate the cut applied for the accepted events.

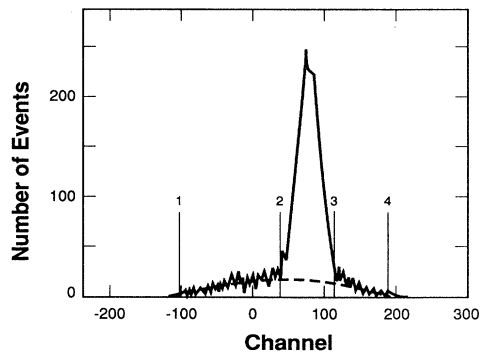

FIG. 4. The coplanarity histograms and corresponding background fit between markers 1 and 4, excluding the region between markers 2 and 3.

B. The background

The largest source of background was quasifree scattering of pions from the bound protons in the target material and the walls of the cryostat. These events appear as a broad distribution in the coplanarity and kinematical histograms due to the Fermi motion of the bound protons. Some of these recoil protons were accepted, giving an unpolarized background under the peak in Fig. 4. A polynomial was fit to the background away from the elastic peak (i.e., between markers 1 and 4 in Fig. 4, excluding the region between markers 2 and 3). The contribution of this fitted background within the acceptance was then evaluated. Backgrounds ranged from 8% to 28% with the higher values for π^+p elastic scattering. The value of the background for example in Fig. 4 is 14.7%. In order not to introduce a false asymmetry when the background is subtracted from good events it must be shown that the background was not polarized. The asymmetries measured for an unpolarized target were $\epsilon_{UD}=0.01\pm0.04$ and $\epsilon_{LR}=0.03\pm0.04$ (statistical error only). The values $\epsilon_{UD}=0.16\pm0.20$ and $\epsilon_{LR}=-0.11\pm0.20$ are the asymmetries of the background events from markers 1 to 2 and 3 to 4 for one particular point when the target was polarized. This supports our assumption that the background is unpolarized.

C. Asymmetry calculation

The polar (θ) and the azimuthal (Φ) angles for a proton scattered in the carbon analyzer are computed at the

TABLE I. Values of the spin-rotation parameters $A(\pm)$ and $R(\pm)$ for π^-p elastic scattering.

$\cos\theta_{c.m.}$	$A(+)$	$A(-)$	$R(+)$	$R(-)$
	Pion beam momentum =427 MeV/c			
−0.792±0.006	116±0.15	1.02±0.15	0.62±0.15	0.18±0.15
−0.833±0.006	0.95±0.13	0.80±0.13	0.82±0.13	0.71±0.13
−0.868±0.006	0.59±0.13	0.68±0.12	0.81±0.12	1.17±0.12
	Pion beam momentum =471 MeV/c			
−0.360±0.011	−0.38±0.12	0.29±0.13	−0.79±0.12	−0.53±0.13
−0.416±0.011	0.03±0.09	0.46±0.11	−1.20±0.09	−0.41±0.11
−0.580±0.009	0.81±0.19	0.22±0.22	−0.68±0.19	0.22±0.21
−0.685±0.009	1.04±0.15	0.83±0.16	0.14±0.15	0.10±0.15
−0.722±0.008	1.10±0.12	0.65±0.10	−0.39±0.13	0.37±0.10
−0.768±0.008	0.98±0.11	0.58±0.09	0.30±0.11	0.62±0.09
−0.808±0.008	0.79±0.11	0.45±0.08	0.75±0.11	0.59±0.08
−0.832±0.006	0.53±0.09	0.77±0.08	0.63±0.09	0.31±0.08
−0.870±0.006	0.42±0.08	0.72±0.08	0.67±0.08	0.66±0.08
−0.902±0.006	0.44±0.08	0.38±0.07	0.65±0.08	1.00±0.07
	Pion beam momentum =547 MeV/c			
−0.127±0.012	−0.64±0.12	−0.94±0.10	−0.24±0.11	−0.45±0.09
−0.190±0.012	−0.25±0.11	−0.83±0.09	−0.04±0.11	−1.01±0.09
−0.385±0.011	−0.57±0.10	−0.50±0.10	0.09±0.10	−0.48±0.10
−0.448±0.011	−0.25±0.09	−0.46±0.09	0.06±0.09	−0.29±0.09
−0.505±0.011	−0.06±0.09	−0.32±0.09	−0.03±0.09	−0.07±0.09
−0.575±0.010	−0.08±0.08	0.41±0.07	0.55±0.08	0.19±0.07
−0.631±0.010	0.20±0.08	0.07±0.07	0.62±0.08	0.39±0.07
−0.677±0.010	0.47±0.08	−0.14±0.07	0.84±0.08	0.55±0.07
−0.827±0.007	0.24±0.07	0.09±0.08	0.90±0.07	0.89±0.08
	Pion beam momentum =625 MeV/c			
0.150±0.012	−0.34±0.17	−0.26±0.16	−0.37±0.16	−0.23±0.15
0.087±0.012	0.17±0.15	−0.65±0.14	−0.54±0.15	−0.50±0.14
−0.026±0.012	−0.75±0.10	−0.53±0.08	−0.28±0.10	−0.23±0.08
−0.082±0.012	−0.75±0.10	−0.81±0.08	−0.30±0.10	−0.27±0.08
−0.161±0.012	−0.58±0.10	−1.08±0.08	−0.33±0.10	−0.48±0.08
−0.266±0.011	−0.95±0.16	−0.58±0.15	−0.03±0.16	0.47±0.15
−0.333±0.011	−0.60±0.15	−0.73±0.14	−0.01±0.15	0.26±0.14
−0.395±0.011	−0.49±0.14	−0.69±0.12	0.12±0.14	0.09±0.12
−0.651±0.009	0.11±0.07	0.28±0.07	0.89±0.07	1.08±0.07
−0.884±0.006	−0.03±0.07	−0.03±0.09	0.98±0.07	0.97±0.09
	Pion beam momentum =657 MeV/c			
−0.840±0.007	0.16±0.14	−0.17±0.12	1.02±0.14	0.95±0.12

point of closest approach of the two tracks in the carbon block. Energy-dependent *p-C* analyzing powers are evaluated as a function of the polar angle in the energy range between 100 and 750 MeV [30,31]. The azimuthal scattering angle determines the up-down ϵ_{UD} and left-right ϵ_{LR} asymmetries, which are computed from the distribution of the events as a function of the azimuthal angle [32] using the weighted-sum method [33,34]. The weighted-sum method uses first-order terms and can eliminate only first-order instrumental asymmetries. Cancellation of higher-order instrumental asymmetries should be accomplished by reversal of the target polarization direction. This follows from Eqs. (16) when the average is taken of results derived by reversing the polarization of the protons incident on the polarimeter. The experiment was designed to take advantage of this cancellation, since the proton polarization in the polarimeter is reversed by reversing the target polarization. This is not

TABLE II. Values of the spin-rotation parameters $A(\pm)$ and $R(\pm)$ for π^+p elastic scattering.

$\cos\theta_{c.m.}$	$A(+)$	$A(-)$	$R(+)$	$R(-)$
	Pion beam momentum =427 MeV/c			
−0.813±0.006	0.83±0.11	1.23±0.14	0.34±0.11	0.16±0.14
−0.853±0.006	0.70±0.11	0.76±0.14	0.93±0.11	0.70±0.13
−0.886±0.006	0.25±0.10	0.80±0.13	0.82±0.09	1.09±0.12
	Pion beam momentum =471 MeV/c			
−0.358±0.011	0.14±0.17	−0.22±0.19	−0.68±0.17	−1.56±0.19
−0.582±0.009	1.18±0.15	0.81±0.17	−0.28±0.15	−0.33±0.17
−0.636±0.009	1.47±0.12	0.81±0.14	−0.07±0.12	−0.10±0.13
−0.685±0.009	1.08±0.12	0.92±0.13	0.43±0.11	0.52±0.12
−0.719±0.008	0.63±0.18	1.07±0.25	−0.13±0.17	0.20±0.23
−0.772±0.008	0.70±0.16	0.82±0.22	0.53±0.15	0.79±0.20
−0.807±0.008	0.47±0.16	0.87±0.22	0.76±0.15	0.35±0.21
−0.832±0.006	0.84±0.09	0.77±0.10	0.46±0.09	0.78±0.10
−0.870±0.006	0.71±0.09	0.51±0.10	0.66±0.09	1.03±0.09
−0.901±0.006	0.57±0.08	0.21±0.09	0.95±0.08	1.00±0.09
	Pion beam momentum =547 MeV/c			
−0.122±0.012	−0.74±0.13	−0.47±0.15	0.62±0.13	0.73±0.15
−0.314±0.011	−1.36±0.24	−0.68±0.16	−0.52±0.24	−0.46±0.16
−0.379±0.011	−0.52±0.21	−0.38±0.14	−0.99±0.21	−0.83±0.14
−0.443±0.011	0.61±0.20	0.14±0.14	−0.86±0.20	−0.81±0.13
−0.416±0.011	−0.40±0.14	0.27±0.16	−0.98±0.15	−0.72±0.16
−0.479±0.011	0.19±0.13	−0.06±0.14	−0.76±0.13	−0.71±0.14
−0.536±0.011	0.59±0.14	0.16±0.15	−0.46±0.14	−0.79±0.15
−0.576±0.010	0.68±0.08	0.77±0.09	−0.14±0.09	−0.28±0.09
−0.621±0.010	0.90±0.08	0.71±0.08	0.33±0.08	0.17±0.08
−0.676±0.010	1.05±0.08	0.44±0.09	0.49±0.08	0.47±0.09
−0.807±0.007	0.75±0.08	0.67±0.07	0.48±0.08	0.63±0.07
−0.848±0.007	0.64±0.08	0.21±0.07	0.76±0.07	0.74±0.06
−0.882±0.007	0.47±0.08	−0.19±0.07	0.81±0.08	0.93±0.07
	Pion beam momentum =625 MeV/c			
0.156±0.012	0.68±0.18	0.49±0.18	0.96±0.17	1.20±0.18
0.089±0.012	0.31±0.16	0.18±0.17	0.85±0.15	0.84±0.16
−0.021±0.012	0.42±0.17	0.30±0.15	1.03±0.17	0.84±0.15
−0.090±0.012	−0.04±0.16	0.30±0.14	0.87±0.17	0.89±0.14
−0.158±0.012	−0.98±0.16	−0.01±0.15	0.88±0.16	1.00±0.15
−0.804±0.006	0.37±0.17	−0.25±0.10	0.84±0.17	0.77±0.10
−0.846±0.006	−0.40±0.18	−0.04±0.10	1.01±0.18	0.60±0.10
−0.879±0.006	−0.61±0.17	−0.05±0.10	1.15±0.17	0.51±0.10
	Pion beam momentum =657 MeV/c			
0.150±0.012	0.99±0.47	0.31±0.19	1.23±0.46	0.85±0.19
0.079±0.012	1.33±0.44	−0.03±0.19	0.89±0.44	1.22±0.19
−0.704±0.008	−0.23±0.15	−0.45±0.19	0.91±0.15	1.16±0.19
−0.755±0.008	−0.33±0.14	−0.90±0.16	0.43±0.14	0.93±0.16
−0.796±0.008	−0.52±0.15	−0.78±0.18	0.55±0.15	0.94±0.18

exactly true for this experiment due to the very small admixture of the N_f component in the calculation of spin-rotation parameters (see Sec. III A).

D. Statistical and systematic uncertainties

The statistical uncertainties have been shown to be [34]

$$\sigma_\epsilon = \left[\frac{2-\frac{3}{2}\epsilon^2}{N} \right]^{1/2} .$$

The symbol ϵ represents either ϵ_{LR} or ϵ_{UD} and N is the number of events. These uncertainties were propagated to A and R for each run using Eqs. (16), with the contributions from ϵ_{LR} and ϵ_{UD} added in quadrature. The total statistical error was then calculated by combining the results for all runs for a given direction of target polarization. For example, this statistical uncertainty for A, σ_A, was calculated from the standard equation

$$\sigma_A = \left[\frac{1}{\sum [1/(\sigma_{A_i})]^2} \right]^{1/2} ,$$

TABLE III. Values of the spin-rotation parameters A and R and the spin-rotation angle β for π^-p elastic scattering.

$\cos\theta_{c.m.}$	A	R	β
	Pion beam momentum =427 MeV/c		
−0.792±0.006	1.09±0.22	0.40±0.22	50.4±6.1
−0.833±0.006	0.88±0.19	0.77±0.18	31.3±5.3
−0.868±0.006	0.64±0.17	1.00±0.21	17.1±5.0
	Pion beam momentum =471 MeV/c		
−0.360±0.011	−0.04±0.27	−0.66±0.21	147.1±5.2
−0.416±0.011	0.25±0.21	−0.81±0.31	128.7±4.2
−0.580±0.009	0.52±0.30	−0.23±0.38	85.5±8.2
−0.685±0.009	0.93±0.19	0.12±0.17	58.1±6.1
−0.722±0.008	0.88±0.21	−0.01±0.28	67.7±4.6
−0.768±0.008	0.78±0.20	0.45±0.18	39.0±4.1
−0.808±0.008	0.62±0.19	0.67±0.15	23.9±3.9
−0.832±0.006	0.65±0.16	0.47±0.19	36.6±3.5
−0.870±0.006	0.57±0.18	0.66±0.15	25.2±3.2
−0.902±0.006	0.41±0.14	0.82±0.19	13.1±3.2
	Pion beam momentum =547 MeV/c		
−0.127±0.012	−0.79±0.21	−0.35±0.16	203.0±4.3
−0.190±0.012	−0.54±0.26	−0.53±0.37	184.3±4.1
−0.385±0.011	−0.54±0.15	−0.20±0.25	214.1±4.0
−0.448±0.011	−0.37±0.16	−0.13±0.18	217.0±3.6
−0.505±0.011	−0.19±0.17	−0.05±0.14	223.0±3.7
−0.575±0.010	0.16±0.22	0.37±0.18	354.7±3.2
−0.631±0.010	0.13±0.15	0.50±0.16	347.9±3.1
−0.677±0.010	0.16±0.26	0.69±0.18	348.1±3.2
−0.827±0.007	0.16±0.15	0.90±0.15	352.2±3.0
	Pion beam momentum =625 MeV/c		
0.150±0.012	−0.29±0.18	−0.30±0.18	172.5±6.5
0.087±0.012	−0.24±0.32	−0.52±0.17	154.7±5.8
−0.026±0.012	−0.64±0.16	−0.26±0.15	201.7±3.8
−0.082±0.012	−0.77±0.15	−0.29±0.15	204.6±3.7
−0.161±0.012	−0.83±0.23	−0.41±0.15	201.0±3.7
−0.266±0.011	−0.77±0.20	0.22±0.23	246.3±6.3
−0.333±0.011	−0.66±0.18	0.13±0.18	243.8±5.8
−0.395±0.011	−0.59±0.17	0.10±0.16	244.3±5.4
−0.651±0.009	0.19±0.15	0.98±0.16	344.5±3.0
−0.884±0.006	−0.03±0.14	0.97±0.15	343.3±3.3
	Pion beam momentum =657 MeV/c		
−0.840±0.007	−0.01±0.21	0.98±0.17	341.9±8.0

TABLE IV. Values of the spin-rotation parameters A and R and the spin-rotation angle β for π^+p elastic scattering.

$\cos\theta_{c.m.}$	A	R	β
	Pion beam momentum =427 MeV/c		
−0.813±0.006	1.03±0.25	0.25±0.16	57.7±5.2
−0.853±0.006	0.73±0.18	0.82±0.19	25.4±4.9
−0.886±0.006	0.52±0.26	0.96±0.20	14.1±4.6
	Pion beam momentum =471 MeV/c		
−0.358±0.011	−0.03±0.21	−1.13±0.41	145.6±7.3
−0.582±0.009	1.00±0.22	−0.31±0.17	78.6±6.3
−0.636±0.009	1.14±0.27	−0.08±0.16	67.3±5.0
−0.685±0.009	1.00±0.16	0.48±0.16	40.0±4.9
−0.719±0.008	0.85±0.24	0.04±0.21	64.5±8.3
−0.772±0.008	0.76±0.19	0.67±0.19	28.0±7.4
−0.807±0.008	0.67±0.21	0.56±0.22	31.3±7.5
−0.832±0.006	0.80±0.17	0.62±0.19	34.6±3.8
−0.870±0.006	0.61±0.16	0.84±0.20	20.3±3.8
−0.901±0.006	0.39±0.18	0.98±0.16	8.3±3.5
	Pion beam momentum =547 MeV/c		
−0.122±0.012	−0.61±0.20	0.67±0.19	274.0±5.7
−0.314±0.011	−1.03±0.33	−0.50±0.20	206.2±8.2
−0.379±0.011	−0.47±0.18	−0.92±0.19	171.8±7.1
−0.443±0.011	0.38±0.26	−0.85±0.18	122.6±7.0
−0.416±0.011	−0.06±0.29	−0.86±0.18	149.6±6.1
−0.479±0.011	0.07±0.19	−0.74±0.17	142.4±5.4
−0.536±0.011	0.38±0.22	−0.63±0.19	118.3±5.9
−0.576±0.010	0.73±0.15	−0.22±0.15	77.5±3.5
−0.621±0.010	0.81±0.16	0.24±0.15	46.4±3.3
−0.676±0.010	0.75±0.26	0.48±0.15	32.3±3.5
−0.807±0.007	0.71±0.15	0.56±0.15	32.5±3.1
−0.848±0.007	0.43±0.21	0.75±0.15	12.6±2.9
−0.882±0.007	0.14±0.26	0.87±0.16	−5.7±3.0
	Pion beam momentum =625 MeV/c		
0.156±0.012	0.58±0.21	1.08±0.25	336.3±7.2
0.089±0.012	0.24±0.18	0.85±0.19	326.1±6.6
−0.021±0.012	0.36±0.18	0.94±0.19	334.0±6.4
−0.090±0.012	0.13±0.18	0.88±0.18	323.6±6.3
−0.158±0.012	−0.50±0.35	0.94±0.18	289.3±6.4
−0.804±0.006	0.06±0.26	0.81±0.18	344.6±5.5
−0.846±0.006	−0.22±0.18	0.81±0.23	327.6±5.9
−0.879±0.006	−0.33±0.25	0.83±0.28	322.9±5.8
	Pion beam momentum =657 MeV/c		
0.150±0.012	0.65±0.31	1.04±0.30	340.0±14
0.079±0.012	0.66±0.52	1.05±0.28	342.3±14
−0.704±0.008	−0.34±0.18	1.03±0.20	317.3±7.0
−0.755±0.008	−0.61±0.26	0.68±0.23	295.8±6.2
−0.796±0.008	−0.65±0.20	0.74±0.23	298.6±6.7

where σ_{A_i} is the uncertainty for the ith run. The total statistical uncertainties for the experiment are such that they contribute from 0.05 to 0.10 to the final uncertainties for A and R.

The total systematic error was calculated again by propagating each systematic error to the final A and R values using Eqs. (16) and then the corresponding uncertainties were added in quadrature. The uncertainties in the determination of the target angle were $\pm 0.5°$, target polarization ± 0.03, and background $\pm 2.0\%$ to $\pm 4.5\%$. The uncertainty in the carbon analyzing power (2–5 %) was calculated from the fit used. The uncertainty of the spin precession matrix B was estimated to be well within $\pm 1\%$ and was not included in the error calculation.

TABLE V. The analyzing power [2] A_N and polarization vector magnitude PVM for $\pi^- p$ elastic scattering.

$\cos\theta_{\text{c.m.}}$	A_N	PVM
Pion beam momentum =427 MeV/c		
−0.792±0.006	0.22±0.06	1.18±0.24
−0.833±0.006	0.18±0.06	1.18±0.20
−0.868±0.006	0.14±0.06	1.19±0.21
Pion beam momentum =471 MeV/c		
−0.360±0.011	0.45±0.10	0.80±0.21
−0.416±0.011	0.58±0.10	1.03±0.32
−0.580±0.009	0.78±0.10	0.96±0.31
−0.685±0.009	0.72±0.10	1.19±0.18
−0.722±0.008	0.68±0.10	1.11±0.19
−0.768±0.008	0.60±0.10	1.08±0.21
−0.808±0.008	0.52±0.10	1.05±0.18
−0.832±0.006	0.46±0.10	0.93±0.19
−0.870±0.006	0.37±0.10	0.95±0.17
−0.902±0.006	0.29±0.10	0.96±0.18
Pion beam momentum =547 MeV/c		
−0.127±0.012	−0.22±0.10	0.89±0.21
−0.190±0.012	0.01±0.10	0.76±0.40
−0.385±0.011	0.83±0.10	1.01±0.17
−0.448±0.011	0.96±0.10	1.04±0.14
−0.505±0.011	0.99±0.10	1.01±0.12
−0.575±0.010	0.93±0.15	1.02±0.21
−0.631±0.010	0.84±0.15	0.98±0.19
−0.677±0.010	0.74±0.15	1.03±0.23
−0.827±0.007	0.43±0.05	1.01±0.10
Pion beam momentum =625 MeV/c		
0.150±0.012	−0.78±0.08	0.89±0.15
0.087±0.012	−0.74±0.08	0.93±0.20
−0.026±0.012	−0.58±0.10	0.91±0.16
−0.082±0.012	−0.45±0.10	0.94±0.14
−0.161±0.012	−0.17±0.10	0.94±0.22
−0.266±0.011	0.36±0.10	0.88±0.22
−0.333±0.011	0.65±0.10	0.93±0.17
−0.395±0.011	0.75±0.10	0.96±0.16
−0.651±0.009	0.23±0.05	1.03±0.12
−0.884±0.006	−0.03±0.05	0.98±0.08
Pion beam momentum =657 MeV/c		
−0.840±0.007	−0.17±0.20	1.00±0.14

V. RESULTS

A. Tabulation

The acceptance angle of the spectrometer in the horizontal plane was about 9°. It was divided into three separate angle bins, as the momentum, the differential cross section, and the analyzing power can change considerably in a 9° wide angular region. Tables I and II

TABLE VI. The analyzing power [2] A_N and polarization vector magnitude PVM for $\pi^+ p$ elastic scattering.

$\cos\theta_{\text{c.m.}}$	A_N	PVM
Pion beam momentum =427 MeV/c		
−0.813±0.006	−0.10±0.05	1.07±0.23
−0.853±0.006	−0.08±0.05	1.10±0.19
−0.886±0.006	−0.07±0.05	1.09±0.24
Pion beam momentum =471 MeV/c		
−0.358±0.011	0.05±0.06	1.13±0.40
−0.582±0.009	−0.18±0.05	1.06±0.21
−0.636±0.009	−0.19±0.05	1.16±0.25
−0.685±0.009	−0.19±0.05	1.12±0.14
−0.719±0.008	−0.19±0.05	0.87±0.21
−0.772±0.008	−0.17±0.05	1.03±0.20
−0.807±0.008	−0.15±0.05	0.89±0.25
−0.832±0.006	−0.14±0.05	1.02±0.18
−0.870±0.006	−0.11±0.05	1.05±0.18
−0.901±0.006	−0.09±0.05	1.06±0.14
Pion beam momentum =547 MeV/c		
−0.122±0.012	0.13±0.10	0.92±0.22
−0.314±0.011	−0.11±0.07	1.15±0.34
−0.379±0.011	−0.26±0.07	1.06±0.20
−0.443±0.011	−0.37±0.07	1.00±0.22
−0.416±0.011	−0.33±0.05	0.93±0.15
−0.479±0.011	−0.41±0.05	0.85±0.13
−0.536±0.011	−0.43±0.05	0.86±0.21
−0.576±0.010	−0.43±0.05	0.88±0.11
−0.621±0.010	−0.41±0.05	0.94±0.13
−0.676±0.010	−0.38±0.05	0.97±0.22
−0.807±0.007	−0.30±0.05	0.95±0.11
−0.848±0.007	−0.27±0.05	0.90±0.15
−0.882±0.007	−0.24±0.05	0.91±0.13
Pion beam momentum =625 MeV/c		
0.156±0.012	−0.02±0.05	1.23±0.26
0.089±0.012	−0.03±0.05	0.88±0.17
−0.021±0.012	−0.05±0.10	1.00±0.18
−0.090±0.012	−0.07±0.10	0.90±0.14
−0.158±0.012	−0.11±0.10	1.07±0.27
−0.804±0.006	−0.34±0.15	0.88±0.18
−0.846±0.006	−0.31±0.15	0.90±0.26
−0.879±0.006	−0.30±0.15	0.94±0.34
Pion beam momentum =657 MeV/c		
0.150±0.012	−0.36±0.20	1.28±0.42
0.079±0.012	−0.33±0.20	1.29±0.51
−0.704±0.008	−0.33±0.20	1.14±0.23
−0.755±0.008	−0.27±0.20	0.95±0.33
−0.796±0.008	−0.22±0.20	1.01±0.28

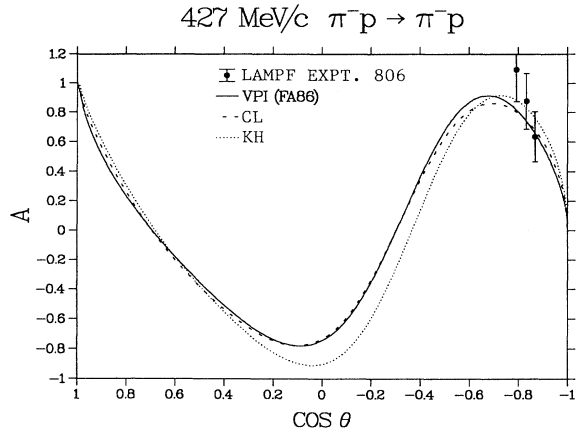

FIG. 5. A for $\pi^-p \to \pi^-p$ at 427 MeV/c.

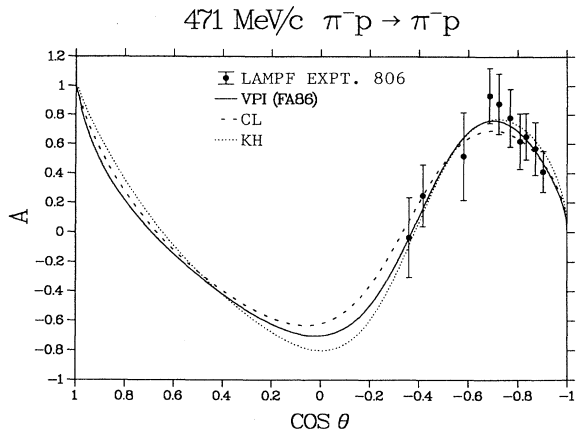

FIG. 7. A for $\pi^-p \to \pi^-p$ at 471 MeV/c.

present our results for the spin-rotation parameters obtained independently for each target polarization: $A(+)$, $A(-)$, $R(+)$, and $R(-)$ [see Eq. (16)]. The errors are statistical ones only.

As can be seen from the tabulation, for several points there are significant discrepancies between the results for the two target polarization directions, well outside the systematic error from sources discussed in Sec. IV D. The discrepancy is presumably due to the higher-order asymmetries which are expected to cancel (see Sec. IV C). We checked this premise by applying pulse height cuts on one of the trigger scintillators in the analyzer software and in that way inducing an artificial asymmetry. For a typical case the values for $A=0.59\pm0.07$, $A(+)=0.60\pm0.09$, $A(-)=0.57\pm0.10$ and $R=0.58\pm0.07$, $R(+)=0.58\pm0.09$, $R(-)=0.58\pm0.10$ (statistical errors only), changed to $A=0.58\pm0.07$, $A(+)=0.74\pm0.09$, $A(-)=0.42\pm0.10$ and $R=0.59\pm0.07$, $R(+)=0.78\pm0.09$, $R(-)=0.40\pm0.10$ for a cut applied to the upper-left scintillator of the four scintillators positioned at the rear of JANUS (BS). The average values A and R agree well, while the results for

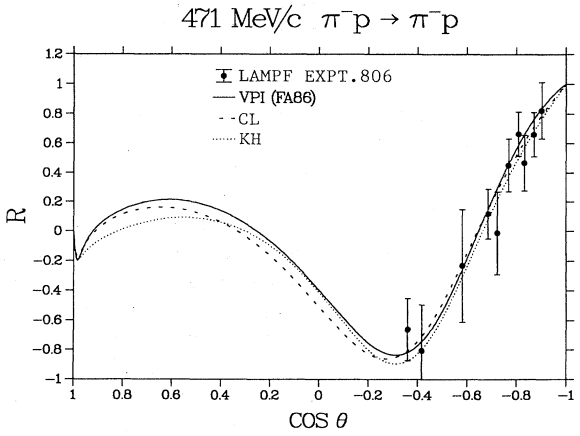

FIG. 8. R for $\pi^-p \to \pi^-p$ at 471 MeV/c.

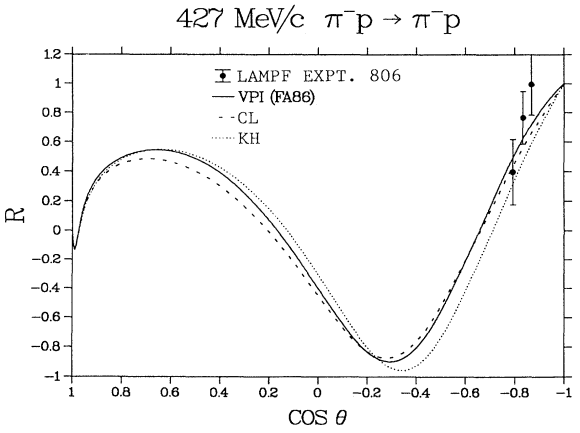

FIG. 6. R for $\pi^-p \to \pi^-p$ at 427 MeV/c.

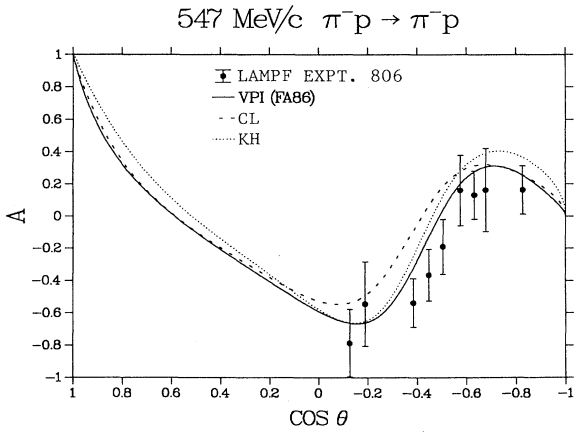

FIG. 9. A for $\pi^-p \to \pi^-p$ at 547 MeV/c.

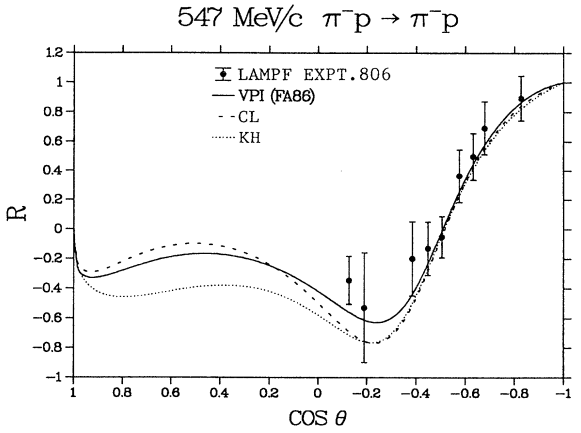

FIG. 10. R for $\pi^- p \to \pi^- p$ at 547 MeV/c.

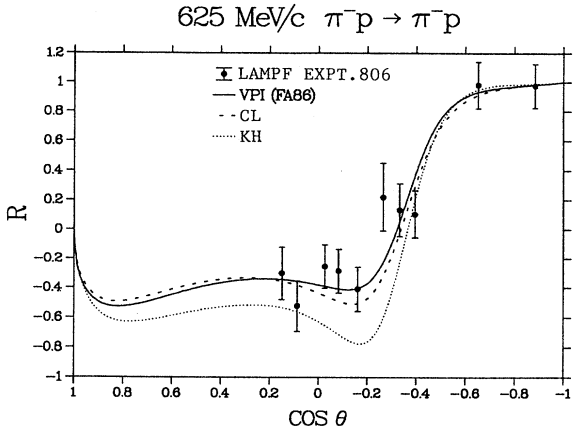

FIG. 12. R for $\pi^- p \to \pi^- p$ at 625 MeV/c.

$A(\pm)$ and $R(\pm)$ changed considerably. An optimistic evaluation of the error would neglect the instrumental uncertainties since the final result is obtained by averaging results from opposite target polarizations. We adopted a more conservative approach. Two standard deviations were calculated, one for the results from all runs combined and one from each group of runs taken from the two target polarizations. When the reproducibility of the results was poor, these standard deviations tended to be higher than the corresponding statistical error. For such cases the average of these two standard deviations was used instead of the statistical error and added in quadrature to the total systematic errors described in Sec. IV D. Also, a weighted root mean square (rms) deviation of $A(\pm)$ and $R(\pm)$ values from the mean values A and R was calculated. The weighting took into account the increased errors for points which had significant differences between the two target polarizations. The rms deviation ranged from 0.10 (in R for π^+ scattering) to 0.17 (in A for π^+ scattering). An average value of 0.13 was used as an overall systematic uncertainty and added in quadrature to the final results. This step more than doubled the

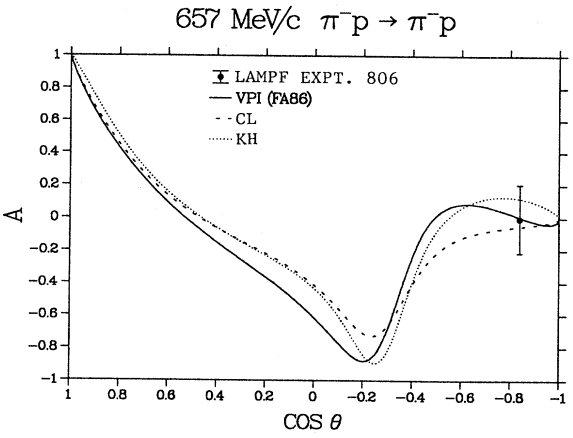

FIG. 13. A for $\pi^- p \to \pi^- p$ at 657 MeV/c.

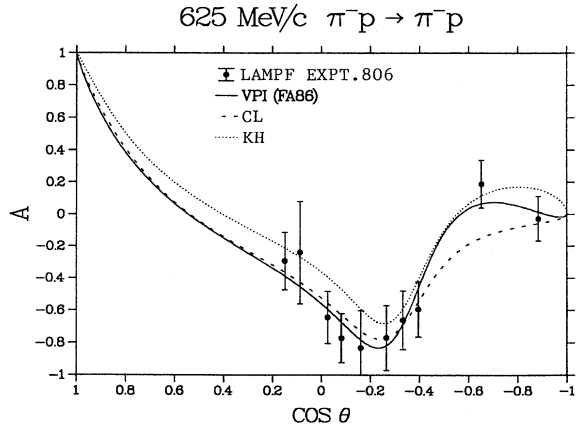

FIG. 11. A for $\pi^- p \to \pi^- p$ at 625 MeV/c.

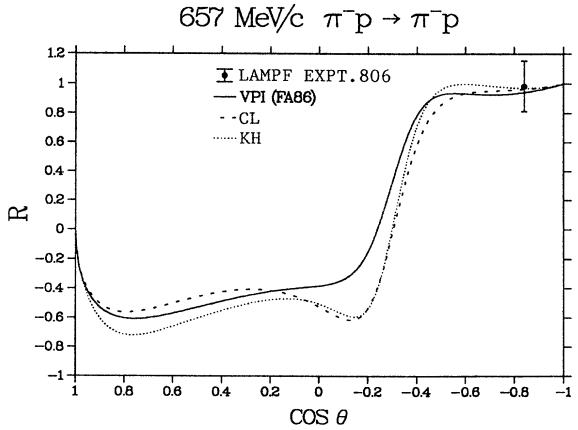

FIG. 14. R for $\pi^- p \to \pi^- p$ at 657 MeV/c.

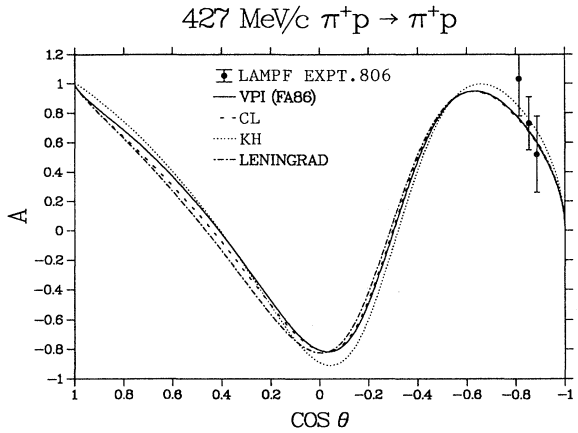

FIG. 15. A for $\pi^+p \to \pi^+p$ at 427 MeV/c.

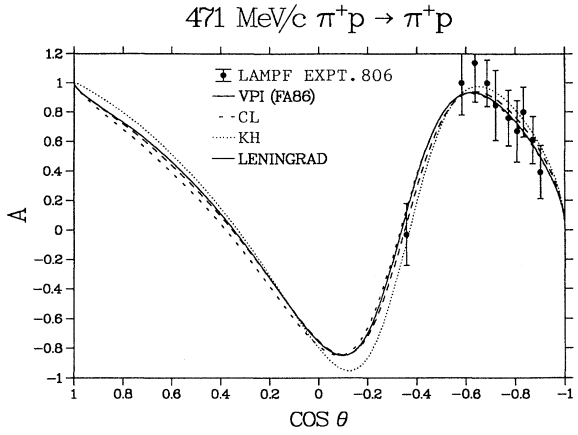

FIG. 17. A for $\pi^+p \to \pi^+p$ at 471 MeV/c.

uncertainties for points which had high statistics and exhibited good consistency of results and had little effect on points whose errors had already been increased due to poor reproducibility of the results.

Our final results for the spin rotation parameters A and R and spin-rotation angle β are presented in Tables III and IV. As β is given by the ratio of A and R, most of the systematic uncertainties cancel, and its error is effectively the statistical error. The values of polarization vector magnitude, PVM$=(A^2+R^2+P^2)^{1/2}$, are calculated by using Eq. (9), where $A_N=P$ (see Sec. III A). They are listed in Tables V and VI along with the fitted values for the analyzing power A_N measured in a previous experiment [2]. Plots of the results for A and R parameters for the full angular acceptance have already been published [35].

B. Comparison to partial-wave analyses

The results are illustrated in Figs. 5–24 and compared with PWA predictions from the VPI, KH, CL, and Leningrad groups. None of these PWA's include our experi-

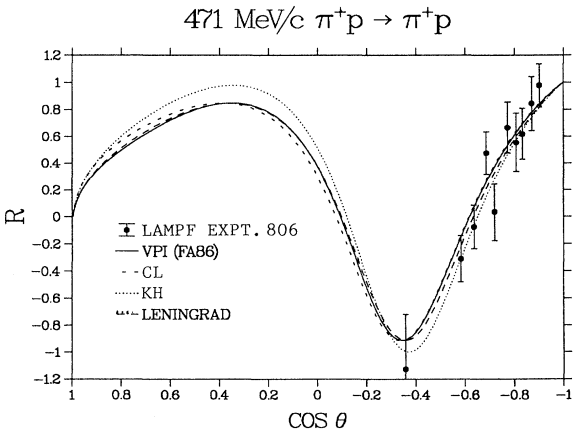

FIG. 18. R for $\pi^+p \to \pi^+p$ at 471 MeV/c.

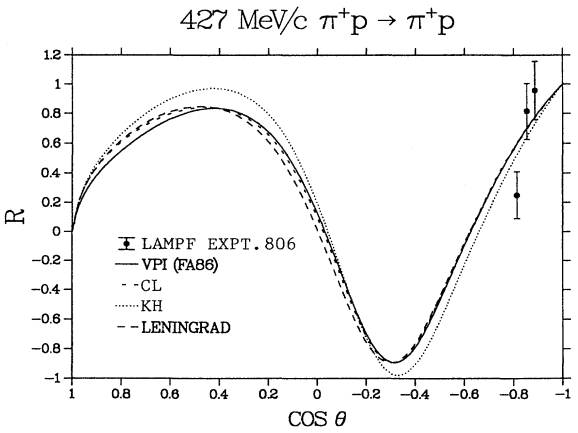

FIG. 16. R for $\pi^+p \to \pi^+p$ at 427 MeV/c.

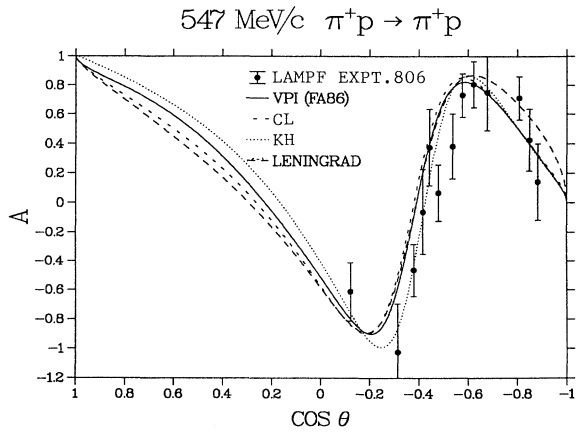

FIG. 19. A for $\pi^+p \to \pi^+p$ at 547 MeV/c.

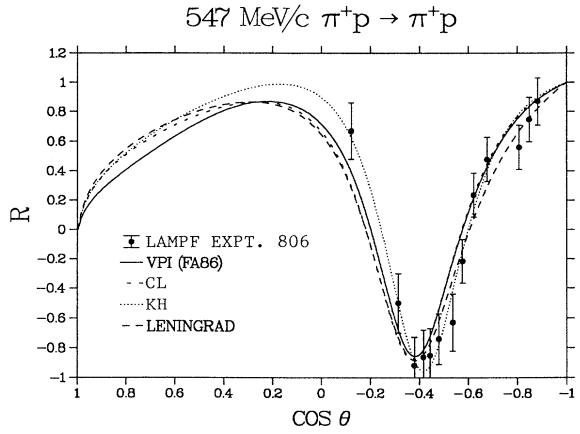

FIG. 20. R for $\pi^+p \to \pi^+p$ at 547 MeV/c.

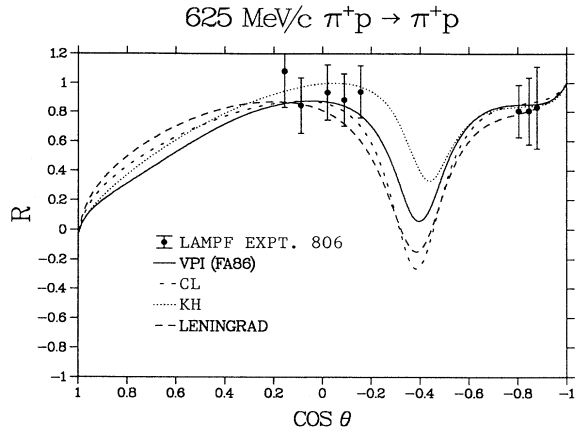

FIG. 22. R for $\pi^+p \to \pi^+p$ at 625 MeV/c.

mental results in their data bases. The only other data on A and R are from the Leningrad group [36]. They are at different beam momenta and the results therefore cannot be compared with ours.

C. Conclusion

The data show good continuity between adjacent or overlapping spectrometer angles, particularly for the R parameter. The R parameter is more sensitive to the instrumental asymmetry in the horizontal plane (left-right). The continuity indicates that binning has not introduced additional asymmetry. The overall consistency of the measurements and normalizations can be tested by checking the polarization vector magnitude (PVM) (see Tables V and VI). The mean PVM value for all the data is 0.99 ± 0.15 and less than 15% of the points deviate more than one standard deviation from one. However, for π^+p at 547 MeV/c and π^-p at 625 MeV/c the PVM's values are systematically lower than the expected value of one. The consistency between the $A(+)$ and $A(-)$ and between $R(+)$ and $R(-)$ results for two target polarization directions give a fair estimate of the JANUS instru-

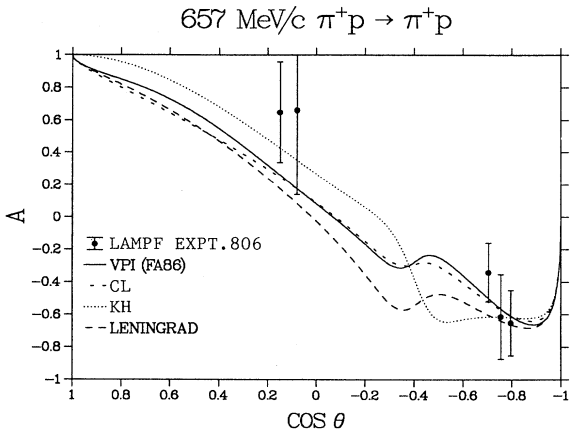

FIG. 23. A for $\pi^+p \to \pi^+p$ at 657 MeV/c.

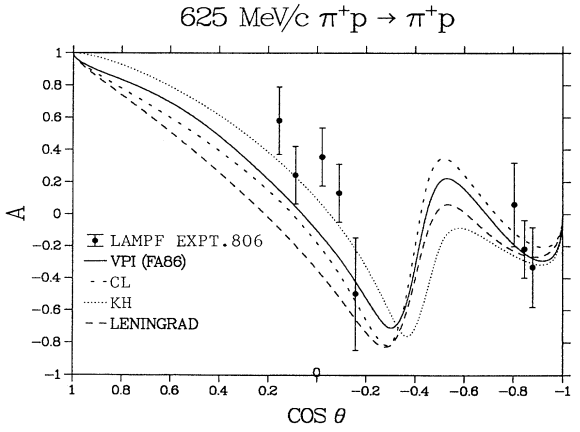

FIG. 21. A for $\pi^+p \to \pi^+p$ at 625 MeV/c.

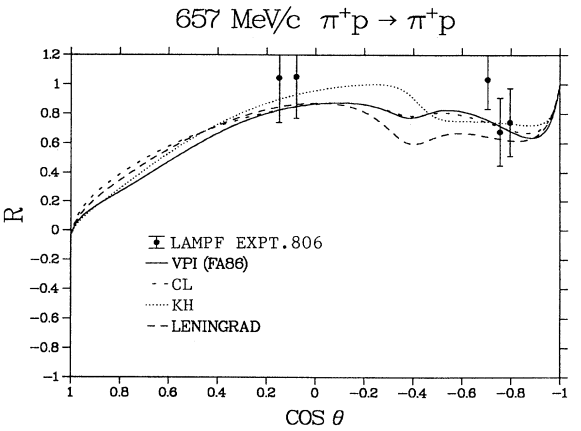

FIG. 24. R for $\pi^+p \to \pi^+p$ at 657 MeV/c.

mental asymmetries. For some points inconsistencies are significant, but should cancel once their values are averaged. Nevertheless, we adopted a conservative estimate of the experimental errors to account for discrepancies in measurements for the two target polarizations.

Results from the present experiment show qualitative agreement with the gross features of the recent πN PWA's up to 657 MeV/c. Some deviation outside the experimental errors indicate the need for a new round of PWA's. When incorporated in new PWA's, these results should provide some insight in the nature of the Roper resonance. Complete data sets now exist at single energies for the first time. Amplitude analyses or single-energy partial-wave analyses can be performed at these energies in order to test the theoretical constraints used in energy-dependent partial-wave analyses. An amplitude analysis can also test the consistency of the data with the assumption of isospin invariance in the πN system.

ACKNOWLEDGMENTS

We are grateful to the LAMPF management, especially L. Agnew, for their support throughout this lengthy experiment, and for the technical assistance such as the construction of the large rotatable target platform and polarimeter stand. This experiment would not have been possible without the contribution from the polarized target group under J. Jarmer. We thank, especially, D. Yeamans and S. Penttila for their dedicated work on the frozen spin target. We appreciate the loan of the proton polarimeter from the LAMPF MP-10 group and the assistance given by M. McNaughton in using it. Special thanks go to S. L. Hall, S. R. Loe, and L. K. Morton (ACU), R. S. Kessler and J. W. Price (UCLA), and S. D. Adrian, L. H. Kramer, and A. M. Petrov (GWU) for their valuable assistance in the experiment and to I. Slaus for help in taking the data.

[1] M. E. Sadler, W. J. Briscoe, D. H. Fitzgerald, B. M. K. Nefkens, and C. J. Seftor, Phys. Rev. D **35**, 2718 (1987).
[2] A. Mokhtari *et al.*, Phys. Rev. D **35**, 810 (1987).
[3] C. J. Seftor *et al.*, Phys. Rev. D **39**, 2457 (1989).
[4] F. O. Borcherding, Ph.D thesis, UCLA, 1982.
[5] J. A. Wightman *et al.*, Phys. Rev. D **38**, 3365 (1988).
[6] G. J. Kim *et al.*, Phys. Lett. B **219**, 62 (1989); Phys. Rev. D **41**, 733 (1990).
[7] N. W. Dean and Ping Lee, Phys. Rev. D **5**, 2741 (1972).
[8] R. A. Arndt, J. M. Ford, and L. D. Roper, Phys. Rev. D **32**, 1085 (1985).
[9] G. Höhler, F. Kaiser, R. Koch, and E. Pietarinen, *Handbook of Pion-Nucleon Scattering* (Fachinformationszentrum, Karlsruhe, 1979); G. Höhler, in *Pion-Nucleon Scattering,* edited by H. Schopper (Springer, Berlin, 1983), Vol. I, 9b2; R. Koch and E. Pietarinen, Nucl. Phys. **A336**, 331 (1980).
[10] R. E. Cutkosky *et al.*, Phys. Rev. D **20**, 2804 (1979); R. E. Cutkosky, C. P. Forsyth, R. E. Hendrick, and R. L. Kelly, *ibid.* **20**, 2839 (1979); updated in *Baryon 1980,* Proceedings of the IVth International Conference on Baryon Resonances, Toronto, edited by N. Isgur (University of Toronto, Toronto, 1981), p. 19.
[11] V. V. Abaev *et al.*, Z. Phys. A **322**, 603 (1985).
[12] Particle Data Group, J. J. Hernández *et al.*, Phys. Lett. B **239**, 1 (1990).
[13] R. J. Eden and J. R. Taylor, Phys. Rev. **133**, B1575 (1964).
[14] R. E. Cutkosky and S. Wang, Phys. Rev. D **42**, 235 (1990).
[15] G. M. Hale, R. E. Brown, and N. Jarmie, Phys. Rev. Lett. **59**, 763 (1987).
[16] N. Isgur and G. Karl, Phys. Rev. D **18**, 4187 (1978); **19**, 2653 (1979); R. Koniuk and N. Isgur, *ibid.* **21**, 1868 (1980).
[17] T. Barnes and F. E. Close, Phys. Lett. **128B**, 277 (1983); E. Golowich, E. Haqq, and G. Karl, Phys. Rev. D **28**, 160 (1983).
[18] M. P. Mattis and M. Karliner, Phys. Rev. D **31**, 2833 (1985); B. Schwesinger, H. Weigel, G. Holzwarth, and A. Hayashi, Phys. Rep. **173**, 173 (1989).
[19] *Higher Energy Polarized Beams (Ann Arbor, 1977),* Proceedings of the Ann Arbor Workshop, edited by A. D. Kirsch and A. J. Salthouse, AIP Conf. Proc. No. 42 (AIP, New York, 1978), p. 142.
[20] A. De Lesquen *et al.*, Phys. Lett. **40B**, 277 (1972).
[21] L. Wolfenstein, Phys. Rev. **96**, 1654 (1954).
[22] G. H. Hohler (private communication); M. E. Sadler *et al.* (unpublished).
[23] R. J. Blin-Stoyle, Proc. Phys. Soc. A **64**, 700 (1951).
[24] P^3 User Group and P. A. M. Gram, LASL Report No. LA-4535-MS, Los Alamos, New Mexico, 1970 (unpublished).
[25] G. J. Krausse and P. A. M. Gram, Nucl. Instrum. Methods **156**, 365 (1978).
[26] P. Autones *et al.*, Nucl. Instrum. Methods **103**, 211 (1972); J. C. Raoul *et al.*, *ibid.* **125**, 585 (1975).
[27] W. de Boer, Nucl. Instrum. Methods **107**, 99 (1973).
[28] J. J. Jarmer and J. Vaninetti, in *Proceedings of the Fourth Workshop on Polarized Target Materials and Techniques,* Bad Honnef, West Germany, 1984, edited by W. Meyer (University of Bonn, Bonn, 1984).
[29] E. Colton, Nucl. Instrum. Methods **178**, 95 (1980).
[30] R. D. Ransome *et al.*, Nucl. Instrum. Methods **201**, 309 (1982).
[31] M. W. McNaughton *et al.*, Nucl. Instrum. Methods A **241**, 435 (1985); E. Aprile-Giboni *et al.*, *ibid.* **215**, 147 (1983).
[32] R. D. Ransome *et al.*, Nucl. Instrum. Methods **201**, 315 (1982).
[33] G. Waters *et al.*, Nucl. Instrum. Methods **153**, 401 (1978).
[34] D. Besset *et al.*, Nucl. Instrum. Methods **166**, 379 (1979); **166**, 515 (1979).
[35] D. B. Barlow *et al.*, Phys. Rev. Lett. **62**, 1009 (1989).
[36] V. S. Bekrenev *et al.*, J. Phys. G **13**, L19 (1987).